

Transforming Small Localized Loading into Large Rotational Motion in Soft Anisotropically Structured Materials

By Stephan Rudykh* and Mary C. Boyce

Actuation of rotational motion in machines and robotics is generally achieved through highly engineered mechanical or electromechanical devices. As the field of soft robotics develops,^[1–9] there is an emerging and expanding need for novel actuation mechanisms. Here, we show the ability to transform small localized loading into large rotational motion via the design of soft anisotropically structured composite materials. The transformation mechanism governing the rotational actuation capitalizes on the underlying coupling of shear and normal modes of stress and strain in anisotropic materials together with the ability of the soft material to locally undergo large deformation.^[10–12] The transformation behavior is further shown to be highly tuneable through selection of the microstructure as demonstrated through simulations and through experiments on multi-material 3D-printed prototypes of soft composite materials with layered microstructures. Figure 1 illustrates the actuation mechanism with a comparison of a homogeneous isotropic soft material to that of layered soft composites in response to a local indentation loading (to be discussed in depth later), depicting the large rotational motions achievable in layered soft composites. The study provides guidelines for designing soft anisotropic materials with tailored performance. The mechanisms of large controllable actuation can be used for macro-, micro-, and nano-actuators and sensors. The findings can be also used for developing simple techniques for obtaining information on anisotropy, and microstructures of materials at small scales.

1. Experiments

Exemplar soft-layered composite materials are fabricated using a multi-material 3D-printer, Objet Connex500. Two photo-sensitive polymeric materials, an acrylic-based photo-

polymer, VeroWhite (VW), and a soft elastomeric material, TangoPlus (TP), are used. The transparent soft matrix is printed in TP (Young's modulus 0.9 MPa), and the stiffer plates are printed in VW (Young's modulus 1.2 GPa). The height of the specimens is $H = 10$ mm, the length is $L = 100$ mm, and the out-of-plane depth is $z = 10$ mm; the thickness of the stiff plates is $t = 0.5$ mm. Prototypes are fabricated with a range in lamination angles relative to the substrate: $\Theta = 0, 15^\circ, 30^\circ, 45^\circ, 90^\circ, 105^\circ$, and 120° ; the volume fraction of the stiff phase is $c = 0.25$. To study the effect of volume fraction, we also fabricate and test composites of $\Theta = 10^\circ$ with different volume fractions of $c = 0.2, 0.3$; and of $\Theta = 110^\circ$ with $c = 0.1, 0.2, 0.3$.

We use indentation loading to induce localized deformation in the specimens. The indentation tests are performed using a Zwick Mechanical Tester. The radius of the cylindrical indenter is 20 mm. The tests are performed quasi-statically with an indenter velocity of 0.1 mm s^{-1} , corresponding to a nominal engineering strain rate of $0.01/\text{s}$. The actuation angle is measured on the right side of the specimens, ϕ_R (see Figure 1); the actuation of the left side is denoted by ϕ_L . In particular, the actuation response of the specimens with lamination angles of ($>180^\circ - \Theta$) on the right side is identical to the actuation response on the left side of specimens with anisotropy angle Θ , $\phi_R(180^\circ - \Theta) = \phi_L(\Theta)$. Representative experiments are shown in Figure 1.

1.1. Numerical Simulations

Finite element (FE) simulations are conducted to examine the behavior of the soft composites with different microstructures (lamination angles, volume fractions). The FE models are verified against the experimental results. The matrix and plates are discretely modeled and taken to be neo-Hookean materials with the experimentally obtained material properties. The materials are assumed to be nearly incompressible, giving shear moduli of $\mu^{(m)} = 0.3 \text{ MPa}$ and $\mu^{(i)} = 0.4 \text{ GPa}$ for the soft matrix and the stiff phase, respectively. FE simulations are also conducted considering a homogenized anisotropic hyperelastic material with a soft shear response, together with a relatively stiff, nearly inextensible direction, and are reported in Appendix C. The cylindrical Indenter and the substrate are essentially modeled to be rigid. The displacement of the Indenter is denoted by Y and it is normalized by the specimen thickness, H , so that the normalized indentation depth is reported as $\Delta = Y/H$.

[*] S. Rudykh

Department of Aerospace Engineering, Technion – Israel Institute of Technology, Haifa, Israel 32000

Department of Mechanical Engineering, Massachusetts Institute of Technology, Cambridge, MA 02139-4307, USA

E-mail: rudykh@mit.edu

M. C. Boyce

School of Engineering and Applied Science, Columbia University, New York, NY 10027, USA

Supporting Information is available from the Wiley Online Library or from the author.

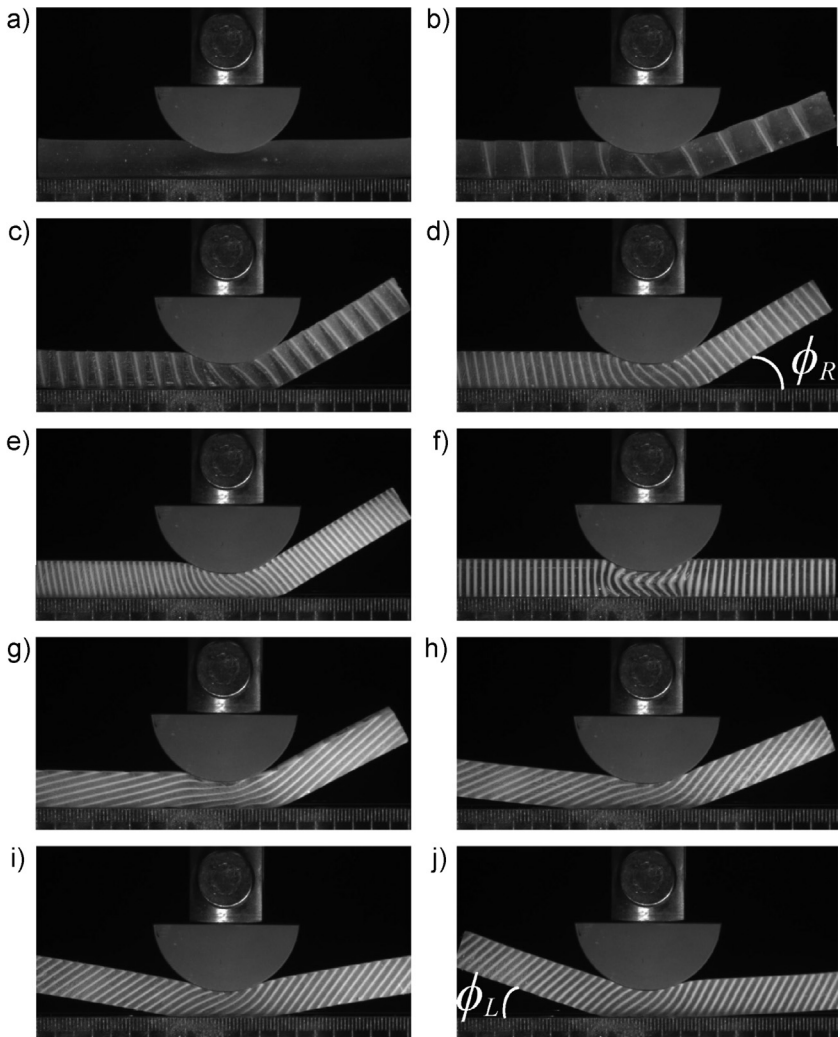


Fig. 1. Soft materials subjected to indentation: (a) homogeneous elastomeric material; (b–e) soft layered composites with anisotropy direction relative to the substrate of $\Theta = 100^\circ$, and stiff phase volume fractions of $c = 0.05$ (b), 0.1 (c), 0.2 (d), and 0.3 (e) and specimens with $c = 0.25$ and with $\Theta = 90^\circ$ (f), 15° (g), 30° (h), 45° (i), and 60° (j). Indentation depth is $Y = 3.9$ mm, specimen height is $H = 10$ mm, and indenter radius is $R = 20$ mm.

2. Results

Figure 1 shows the responses to an indentation of a homogeneous elastomeric material (a), and anisotropically structured soft composite materials. In both isotropic and anisotropic materials, the deformation is mostly localized near the indentation area (Figure 1a). However, the anisotropically structured soft-layered composites transform the localized deformation beneath the indenter into a global rotational motion of the portion of the specimen extending out from the side of the indenter region. Composites with anisotropy directions $\Theta = 100^\circ$ and volume fractions of the stiffer phase $c = 0.05$ (b), 0.1 (c), 0.2 (d), 0.3 (e) show significant actuation on the right side of the specimen. By changing the lamination angle, the actuation on the left, right, or both sides can be achieved (see the performance of composites with $c = 0.25$ and with $\Theta = 90^\circ$ (f), 15° (g), 30° (h), 45° (i), and 60° (j)). The case of aligned loading and anisotropy, $\Theta = 90^\circ$ (f),

does not result in the local-to-global transformation mechanism, and the loading is localized by a local layer buckling mechanism similar to that observed in macroscopic compression.^[13]

FE simulations are used to reveal more details of the mechanisms governing the actuation. Figure 2 shows a comparison of experiments and FE simulation results. We plot normalized force $f = F/(uzH)$ as a function of the indentation depth, Δ . The results are presented separately for composites with small lamination angles in Figure 2a and for large lamination angles in Figure 2b, also including the experimental and FE results for the homogeneous isotropic case. FE simulation results are denoted by continuous curves and the experiments are represented by dotted curves. We note an excellent agreement between the model and experimental results. For small lamination angles (Figure 2a), the slope (the rate of increase of force with an increase in indentation depth) clearly increases with indentation depth. For 30° laminate, an indentation results in significant shearing of the matrix between plates (as will be shown later), and, hence, a lower indentation force than for 15° lamination angle is observed. For the high lamination angles (Figure 2b) close to 90° , we observe an initially stiffer response (see the laminate with 105° in Figure 2b), which then significantly softens (i.e., the tangent stiffness dramatically decreases) as the indentation depth increases; the decrease in stiffness occurs due to the onset of buckling and/or bending of the plates (as shown next).

Figure 3a shows the dependence of the right actuation angle, ϕ_R , on the normalized indentation depth, Δ , for composites with $c = 0.25$ and various lamination angles. The actuation angle was obtained from FE simulations. (Additionally, the potential “lifting force” associated with this actuation was also computed and is reported in Appendix A.) The actuation angle monotonically increases with an increase in indentation depth for all cases. Composites with large lamination angles (close to 90°) exhibit higher actuation angles as a response to a localized loading, but they also show a decreasing slope, i.e., a decrease in the increment in rotation achieved with an increase in indentation. In contrast, composites with small lamination angles, less than 45° , do not show a decrease in the slope. Thus, at a sufficiently large indentation depth, these curves intersect and the composites with initially lower actuations now demonstrate larger actuation in response to similar localized loadings. For example, at the indentation depth, $\Delta = 0.1$, the composites with $\Theta = 100^\circ$ (red dashed curve) and $\Theta = 12^\circ$ (blue

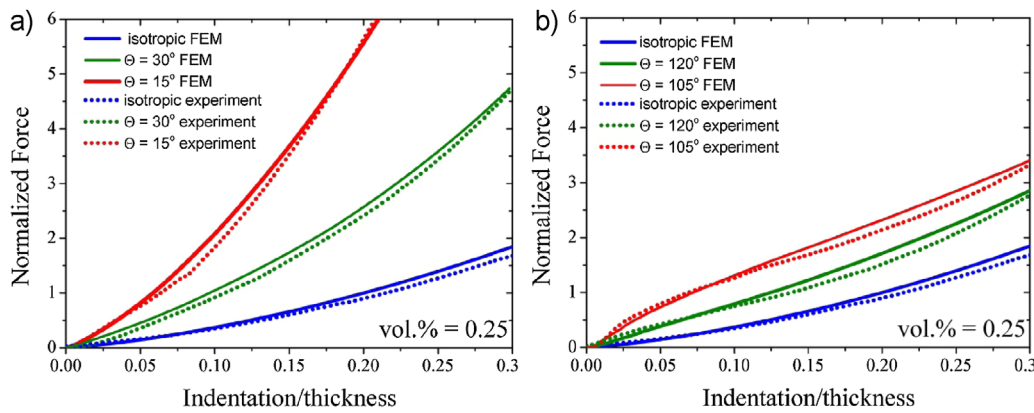


Fig. 2. Comparison of experimental and FE simulation results for dependence of the applied force on indentation depth for composites with $c = 0.25$ and different lamination angles: $\Theta = 15^\circ$ and 30° (a); $\Theta = 105^\circ$ and 120° (b).

continuous curve) are actuated to $\phi_R = 12^\circ$ and 8.2° ; however, when subjected to the localized load of $\Delta = 0.3$, they show $\phi_R = 31^\circ$ and 26.3° , respectively. The actuation of the left side is $\phi_L = 0$ for these composites. The corresponding actuation of the isotropic material is $\phi_R = \phi_L = 2.15^\circ$ and 7.12° for $\Delta = 0.1$ and $\Delta = 0.3$, respectively. The rotational actuation (and its dependence on the lamination angle) is a result of the different micromechanical mechanisms in materials with large and small lamination angles. For composites with large lamination angles, the localized load causes a shearing of the soft matrix which, due to the relative inextensibility of the plate direction, gives rise to rotation of the relatively stiff material direction (i.e., the direction of the plates) as seen both the bending and the rotation of the plates at the region of the indentation. In parallel, a convex bending (and downward rotation) occurs to the left of the indentation center and a concave bending (and

upward rotation) occurs to the right, accompanied by shearing of the matrix between the plates (Figure 3c, e, and h). The concave bending on the right actuates the lifting or rotation of the right side while the convex bending does not lead to lifting of the left side. Hence, the asymmetry in rotational actuation is achieved. For the case of the small lamination angles, a localized matrix shear accompanied by convex bending of the long plates occurs beneath the indenter and in the region of the plates to the right. The combination of the matrix shearing and the plate rotation and bending acts to lift the right side of the specimen (Figure 3b, d, and g). Additional schematics of the actuation mechanism for composites with small and large lamination angles are shown in Figure 4. The actuation behavior is also evident in homogenized anisotropic materials that consist of a relatively compliant shear stiffness combined with a relatively stiff (i.e.,

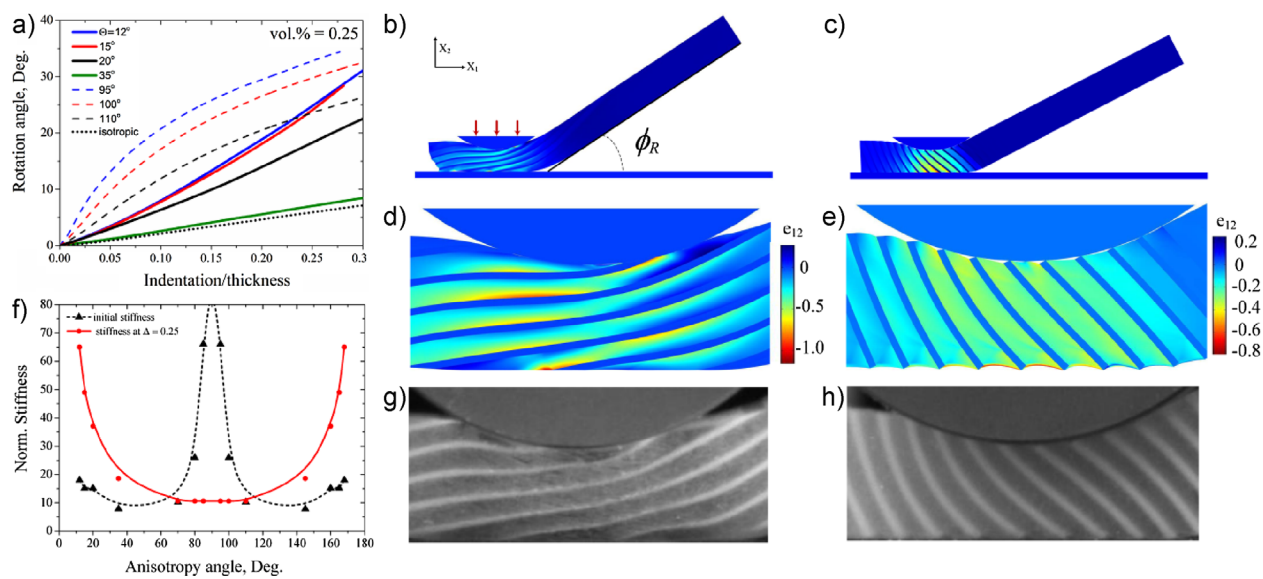


Fig. 3. (a) Actuation angle versus normalized indentation depth (indentation/specimen thickness) for composites with $c = 0.25$ and different lamination angles; (b) and (c) actuated composites with lamination angle $\Theta = 12^\circ$ (b) and $\Theta = 105^\circ$ (c); indentation depth is 3.2 mm. Local deformations at indentation depth is 2.5 mm: (d) and (e) – shear strain distributions FE simulations; (g) and (h) – experiments. Panels (b), (d), and (e) for $\Theta = 12^\circ$, (c), (e), and (h) for 105° . (f) Stiffness versus lamination angle; black curve is for initial stiffness at $\Delta = 0.01$; red curve for stiffness at $\Delta = 0.25$.

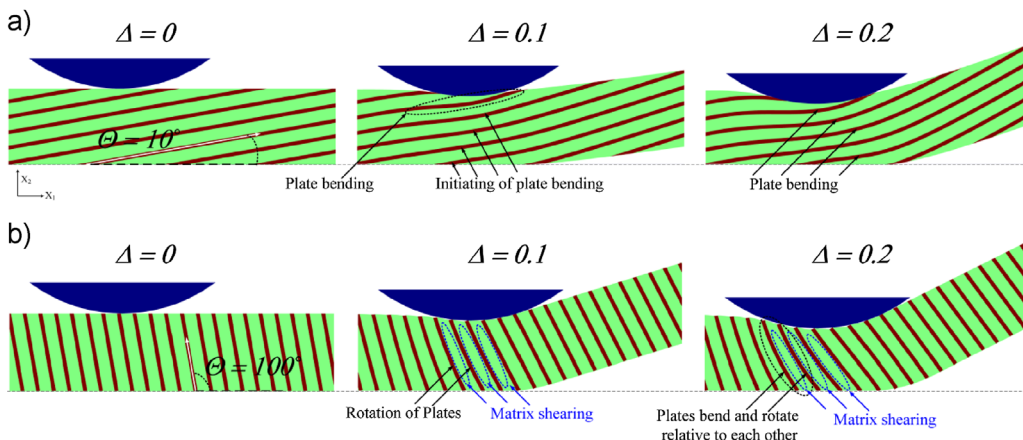


Fig. 4. Schematics of actuation mechanism for composites with $c = 0.25$ and $\Theta = 10^\circ$ (a) and $\Theta = 100^\circ$ (b). The actual matrix shearing can be observed in Figure 3d and e.

relatively inextensible) material direction, as shown in Appendix B – further verifying the role of the effective anisotropy of the soft material composite structure in giving rise to this actuation behavior.

Note that there is a transition from the actuation mechanisms observed for small and large lamination angles; with an increase of lamination angle toward $\Theta \sim 45^\circ$, the composite response to the indentation becomes similar to that of the isotropic material, and, hence, a significant reduction in the actuation is observed (see, e.g., the curve for $\Theta = 35^\circ$ in Figure 2a). A further increase in the lamination angle, past $\Theta \sim 45^\circ$, leads to the actuation mechanism observed in composites with large lamination angles.

We note that there is no significant deformation (i.e., no shearing of the matrix) within the actuated side of the specimen; the deformation is localized under the indenter area (see Figure 1). Clearly, the anisotropic structure is only needed locally in the indentation region to achieve the global rotational actuation; however, anisotropy along the entire length enables the creation of multiple localized loadings and/or loadings that move along the length to control the location and nature of the actuation.

The stiffness of the composites with large and small lamination angles is shown in Figure 3f, presenting the

dependence of the tangent stiffness on lamination angle at $\Delta = 0.01$ (black triangles), and at $\Delta = 0.25$ (red circles); $c = 0.25$. Initially, composites with large anisotropy angles are significantly stiffer because the indentation requires local compression of the stiff plates. However, the deformation mechanism changes with increasing indentation, such that the stiff direction (i.e., the direction of the plates) starts to rotate, avoiding direct compressive strain, and the deformation is: one of the plates bending, and localized shear in the soft matrix (see Figure 3e). Composites with small anisotropy angles possess long stiff layers, and hence the large localized loading causes significant cooperative matrix shear and bending of the stiff layers (see Figure 3d). At large indentation depths, composites with small lamination angles exhibit large tangent stiffness due to the large forces that are required for the cooperative bending of the stiff plates.

The influence of phase volume fraction on the material performance is shown in Figure 5, giving the dependence of actuation angle (Figure 5a and b) on normalized indentation depth as a function of volume fraction for composites with lamination angles $\Theta = 10^\circ$ (Figure 5a) and $\Theta = 100^\circ$ (Figure 5b). The actuation angle is obtained from FE simulations. The dotted curve corresponds to the isotropic material and it shows the lowest actuation. Significant

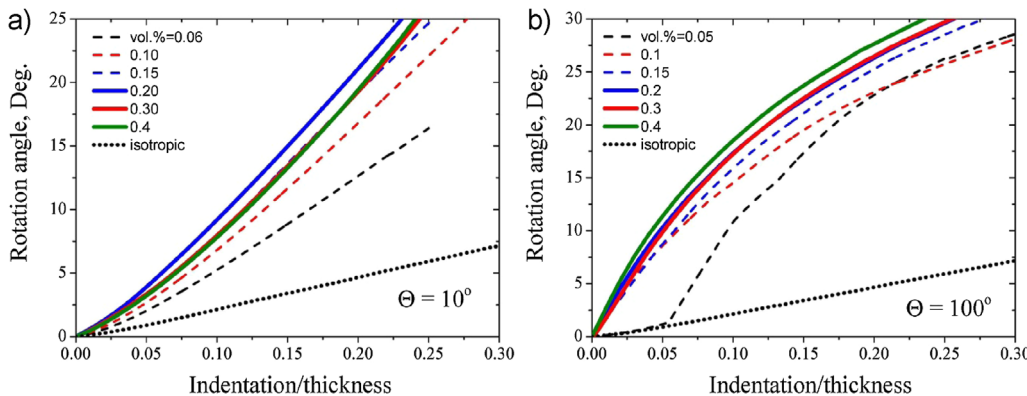


Fig. 5. Actuation rotation angles versus indentation depth for composites with $\Theta = 10^\circ$ (a) and $\Theta = 100^\circ$ (b), and different volume fractions of the stiffer phase.

actuation of rotation is observed to occur with relatively small volume fraction (6%) as long as the deformation mechanism can be achieved beneath the indenter (i.e., plates are present beneath the indenter). A further increase in the volume fraction results in more rapid actuation of rotation with indentation; that continues until about $c=0.15$, where an increase in volume fraction does not significantly change the actuation (see Figure 5a). The tendency is similar for composites with large lamination angles (Figure 5b).

Figure 6a shows the dependence of the tangent stiffness on volume fraction at $\Delta=0.01$ and at $\Delta=0.25$ for $\Theta=10^\circ$ and for $\Theta=100^\circ$. The tangent stiffness is obtained from FE simulations. A significant increase in stiffness is observed with an increase of volume fraction for cases where the actuation mechanism is activated (Figure 6a). The effect is more pronounced in composites with small lamination angles at the indentation depths where the plate bending is significant. The corresponding distributions of shear strain in the indentation area are presented in Figure 6b, c, f, and g for $\Theta=10^\circ$ and for 100° – (Figure 6d, e, h, and i); Figure 6b–e for $\Delta=0.01$; Figure 6f–i for $\Delta=0.25$. Volume fractions are $c=0.05$ – Figure 6a and f; $c=0.06$ – Figure 6d and h; $c=0.4$ – Figure 6c, e, g, and h. We observe that for composites with $\Theta=10^\circ$, finite indentation ($\Delta=0.25$) results in significant bending of the stiff plates, which is the reason for the significant difference in the initial and finite stiffness of these composites. For composites with large lamination angles, the difference in initial and finite stiffness is not that significant because, after the actuation mechanisms are triggered, the plates rotate, and the deformation is mostly accommodated in the soft matrix (see, e.g., Figure 6h).

Through experiments and numerical simulations, we presented soft anisotropically structured materials capable of transforming localized loadings into large rotational movement. The combination of the soft matrix that is capable of sustaining extremely large local shearing, and stiff plates that are capable of buckling and bending, gives rise to the

ability of the local-to-global actuation transformation. The global actuation is highly tunable by the microstructure parameters (lamination angle and volume fraction) as well as by deformation.

3. Appendix A: Dependence of Lifting Force on Microstructure Parameters

The anisotropically structured materials can exert forces on the lifting sides as a response to a local actuation. The potential lifting force is determined by constraining the rotation of the actuated side and calculating the net constraint force. The reported lifting force is normalized by the coefficient μHl , where l is the length of the constrained surface. To illustrate the dependence of the lifting force on the microstructure parameters, in Figure 7, we plot the lifting force as a function of the indentation depth for composites with small and large lamination angles and different volume fractions of the stiff phase. Clearly, the lifting force increases with an increase in volume fraction. Also, the exerted force increases with an increase in indentation depth. However, this increase is different for small (Figure 7a) and large (Figure 7b) angles. In particular, the composites with large lamination angles show a flattening of the curves at some indentations, and consequently, the lifting force that can be exerted is limited for these composites. This behavior is not observed for composites with large lamination angles, for which the lifting force increases nearly linearly with the indentation depth.

4. Appendix B: Dependence of Actuation on Indenter Size

To illustrate the dependence of the actuation on the indenter size, in Figure 8, we plot the rotation angle as a function of the normalized indenter radius, R/H , for composites with small and large lamination angles and with $c=0.3$. For small lamination angles (Figure 8a), we observe that the actuation angle increases slightly with an increase in

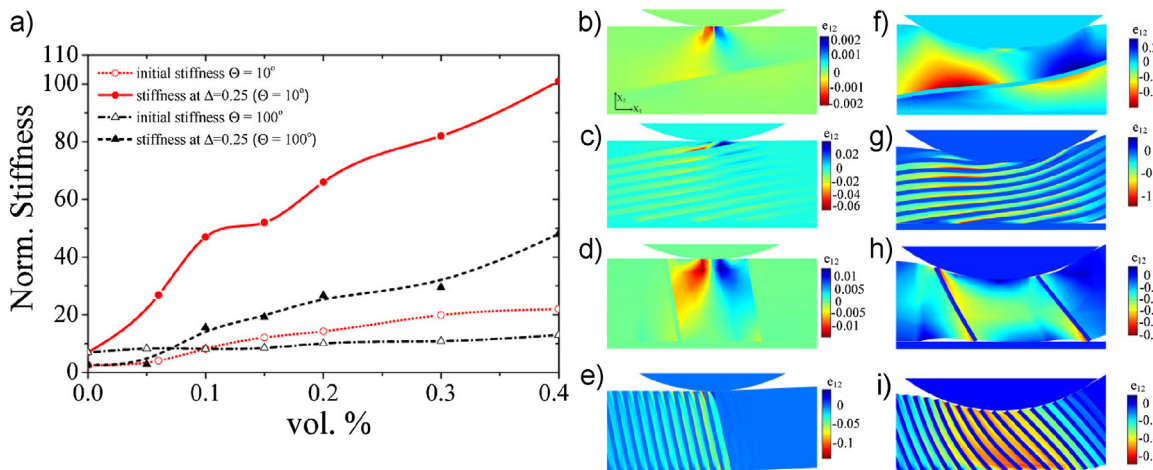


Fig. 6. (a) Stiffness versus volume fraction; red dash-dotted and black dotted curves for initial stiffness at $\Delta=0.01$; black dashed and red continuous curves for stiffness at $\Delta=0.25$. Shear strain distributions for $\Theta=10^\circ$ – (b), (c), (f), and (g); for 100° – (d), (e), (h), and (i); (b), (c), (d), and (e) for $\Delta=0.01$; (f), (g), (h), and (i) for $\Delta=0.25$. Volume fractions are $c=0.05$ – (a) and (f); $c=0.06$ – (d) and (h); $c=0.4$ – (c), (e), (g), and (h).

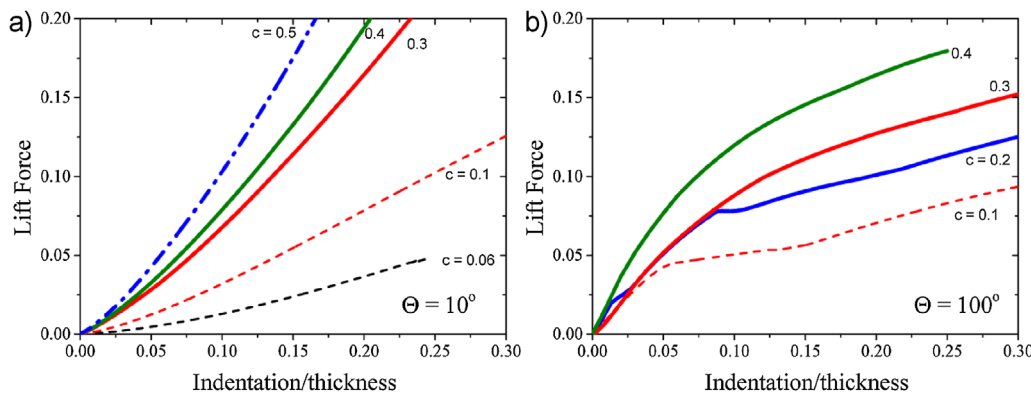


Fig. 7. Lift force versus indentation depth for (a) $\Theta = 10^\circ$ and (b) $\Theta = 100^\circ$ and various volume fractions.

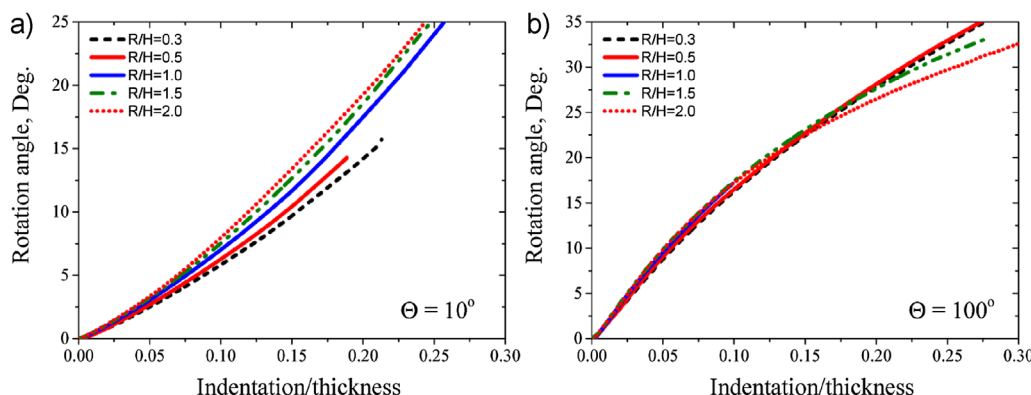


Fig. 8. Rotation angle versus indentation depth for composites with $c = 0.3$ and (a) $\Theta = 10^\circ$ and (b) $\Theta = 100^\circ$ and various radius of indenter.

the radius of the indenter. However, for composites with large lamination angles (Figure 8b), a change in the actuation with an increase of the indenter size is not significant. Moreover, for these composites at large indentation depth, the actuation angle will be large for smaller indenters.

5. Appendix C: Actuation of Homogeneous Anisotropic Material

To highlight the role of anisotropy in the actuation mechanism, we show responses of *homogeneous anisotropic* materials to indentation. We define the material properties through a modified energy density function of deformation, $W = \mu(\mathbf{f}/2)(I_1 - 3) + \beta(I_4 - 1)^2$, where I_1 is the first invariant of right Cauchy deformation tensor $\mathbf{C} = \mathbf{F}^T \mathbf{F}$, and $I_4 = (\mathbf{C} \mathbf{N}) \cdot \mathbf{N}$ represents the anisotropy in the direction \mathbf{N} . Thus, β is the

coefficient that defines the anisotropy of the material. Obviously, when $\beta = 0$, the material behavior is described by isotropic the neo-Hookean model. Here, we present the examples of actuation for $\beta = \mu$, where the anisotropy directions are (a) $\Theta = 15^\circ$ and (c) $\Theta = 75^\circ$ (see Figure 9). The responses of the corresponding layered materials are presented in Figure 9b and d for $\Theta = 15^\circ$ and $\Theta = 75^\circ$, respectively, with colors representing normalized energy-density, $\Psi = W/(\mu^{(m)} z)$. Clearly, the introduced anisotropy gives rise to different actuations of these materials, in particular the material with $\Theta = 15^\circ$ exhibits actuation of the right side, while the specimen with $\Theta = 75^\circ$ shows actuation of the left side. The dependence of the actuation is similar to that observed for the anisotropically structured layered material, but in this case the coupling is defined by an arbitrary coefficient β , rather than a volume fraction in the

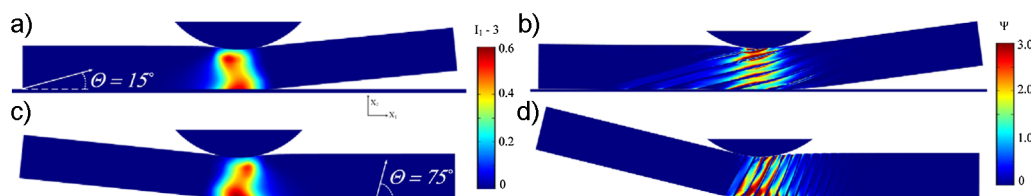


Fig. 9. Actuation of anisotropic homogeneous composites with anisotropy angles (a) $\Theta = 15^\circ$ and (c) $\Theta = 75^\circ$; $\Delta = 0.91$. Colors represent a measure of deformation distribution, $I_1 - 3$. Response of corresponding layered composites is for lamination angles (b) $\Theta = 15^\circ$ and (d) $\Theta = 75^\circ$, $c = 0.25$. Colors represent normalized strain energy-density distribution.

case of the composites. We note, that consistent with the previous observation, the deformation occurs mostly in the area beneath the indenter (see the color distribution of a deformation measure, (I_1 –3), in Figure 9).

Received: February 1, 2014

Final Version: April 29, 2014

Published online: June 30, 2014

- [1] G. Sumbre, G. Fiorito, T. Flash, B. Hochner, *Nature* **2005**, *433*, 7026.
- [2] R. V. Martinez, C. R. Fish, X. Chen, G. M. Whitesides, *Adv. Funct. Mater.* **2012**, *22*, 1376.
- [3] S. A. Morin, R. F. Shepherd, S. W. Kwok, A. A. Stokes, A. Nemirovski, G. M. Whitesides, *Science* **2012**, *337*, 6096.
- [4] R. V. Martinez, J. L. Branch, C. R. Fish, L. Jin, R. F. Shepherd, R. Nunes, Z. Suo, G. M. Whitesides, *Adv. Mater.* **2013**, *25*, 205.
- [5] E. T. Roche, R. Wohlfarth, J. T. B. Overvelde, N. V. Vasilyev, F. A. Pigula, D. J. Mooney, K. Bertoldi, C. J. Walsh, *Adv. Mater.* **2014**, *26*(8), 1200. doi: 10.1002/adma.201304018.
- [6] M. D. Bartlett, A. B. Croll, D. R. King, B. M. Paret, D. J. Irschick, A. J. Crosby, *Adv. Mater.* **2012**, *24*, 1078.
- [7] R. F. Shepherd, A. A. Stokes, R. M. D. Nunes, G. M. Whitesides, *Adv. Mater.* **2013**, *25*, 6709.
- [8] H. Okuzaki, T. Kuwabara, K. Funasaka, T. Saido, *Adv. Funct. Mater.* **2013**, *23*, 4400.
- [9] L. Ionov, *Adv. Funct. Mater.* **2013**, *23*, 4555.
- [10] A. Browning, C. Ortiz, M. C. Boyce, *J. Mech. Behav. Biomed. Mater.* **2012**, *19*, 75.
- [11] S. Rudykh, M.C. Boyce, *IMA J. Appl Math.* **2014**, doi: 10.1093/imamat/hxu005.
- [12] S. Rudykh, M. C. Boyce, (MIT) USA 61/881022. **2013**.
- [13] Y. Li, N. Kaynia, S. Rudykh, M. C. Boyce, *Adv. Eng. Mater.* **2013**, *15*(10), 921.